

## An optimization method with precomputed starting points for solving the inverse Mie problem

This article has been downloaded from IOPscience. Please scroll down to see the full text article.

2012 Inverse Problems 28 045012

(<http://iopscience.iop.org/0266-5611/28/4/045012>)

View [the table of contents for this issue](#), or go to the [journal homepage](#) for more

Download details:

IP Address: 194.85.127.65

The article was downloaded on 30/03/2012 at 03:34

Please note that [terms and conditions apply](#).

# An optimization method with precomputed starting points for solving the inverse Mie problem

G V Dyatlov<sup>1,2</sup>, K V Gilev<sup>2,3</sup>, M A Yurkin<sup>2,3</sup> and V P Maltsev<sup>2,3</sup>

<sup>1</sup> Sobolev Institute of Mathematics, Koptyug Avenue 4, Novosibirsk 630090, Russia

<sup>2</sup> Novosibirsk State University, Pirogova 2, Novosibirsk 630090, Russia

<sup>3</sup> Institute of Chemical Kinetics and Combustion, Institutskaya 3, Novosibirsk 630090, Russia

E-mail: [maltsev@kinetics.nsc.ru](mailto:maltsev@kinetics.nsc.ru)

Received 27 December 2010, in final form 6 March 2012

Published 29 March 2012

Online at [stacks.iop.org/IP/28/045012](http://stacks.iop.org/IP/28/045012)

## Abstract

We study the inverse light-scattering problem which arises in the characterization of small particles by means of scanning flow cytometry. The problem is stated in general form as the problem of solution of a nonlinear equation and solved by the gradient optimization method. In this event, the problem of choosing the starting point appears. In this paper, we propose a method for making this choice based on the preliminary analysis of the direct map. A number of numerical examples are given, using both synthetic and experimental data.

## 1. Introduction

This paper is devoted to the issues connected with the solution of nonlinear equations by gradient methods. Such equations appear in numerous applied problems, in particular, in the characterization of small particles by means of scanning flow cytometry. This problem has served as the main motivation of the present research.

Scanning flow cytometry has been used for the characterization of blood and other particles for more than a decade. We consider the specific statement connected with using the scanning flow cytometer designed at the Institute of Chemical Kinetics and Combustion, Novosibirsk, Russia. A detailed description of the cytometer is given in [1].

Mathematically, the existing version of the cytometer measures the light-scattering pattern (LSP):

$$A(\theta) = \frac{1}{2\pi} \int_0^{2\pi} (S_{11}(\theta, \varphi) + S_{14}(\theta, \varphi)) d\varphi, \quad 10^\circ \leq \theta \leq 70^\circ, \quad (1)$$

where  $S_{ij}(\theta, \varphi)$  are the entries of the Muller matrix (see section 2). For spherically symmetric particles  $S_{14} \equiv 0$ .

As a rule, data for the solution of the inverse light-scattering problem acquired in real experiments are usually incomplete. First, this is caused by the impossibility of measuring the

phase of the wave, except for microwave-analogue experiments [2]. It means that we usually have only the Muller matrix  $S_{ij}(\theta, \varphi)$  rather than the amplitude matrix  $S_i(\theta, \varphi)$  (see section 2). Second, it is not always possible to measure all entries  $S_{ij}(\theta, \varphi)$ . Third, it is practically impossible to obtain the scattering data in the directions close to the incident and backward directions. The difficulties listed are typical of all inverse scattering problems. In our case, an additional loss of information happens due to integration over the azimuth angle  $\varphi$ . All these circumstances complicate the purely theoretical study of the problem and construction of practically usable inversion algorithms.

By the characterization problem we mean the problem of finding the shape and size of a particle and (possible) its internal structure. In practice, we deal with specific particles which can be described by a few parameters. On the other hand, we have finitely many data, though their number can be much greater than the number of parameters.

Using the Maxwell equation (see section 2), for given parameters we can find the scattering data, i.e. construct the map  $f$  such that

$$(A(\theta_1), \dots, A(\theta_m)) = f(x_1, \dots, x_n), \quad (2)$$

where  $x_i$  are the parameters of the particle.

Thus, we need to solve a nonlinear equation with the known map  $f$ . Considering the difficulty of the direct problem and complications connected with the incompleteness of data, we can hardly hope to invert  $f$  theoretically and obtain an explicit inversion formula. Therefore, it is more realistic to seek a solution by an optimization method, minimizing the residual functional. However, as the numerical simulations show, in our case the residual has many local minima which leads to the necessity of choosing a good starting point. In this paper, we propose a method for choosing the starting point based on the preliminary analysis of the direct map  $f$ . Note that in flow cytometry it is necessary to process large samples of similar particles. The proposed approach assumes that the preliminary analysis is carried out once for the whole sample, given the parameters' ranges. Then, the single set of starting points can be used for all particles in the sample.

As an example of application, we consider the simplest problem of finding the radius and refraction index of a spherical particle from the LSP  $A(\theta_j)$  measured at finitely many angles  $\theta_j, j = 1, \dots, m$ .

The paper is organized as follows. In section 2, we give necessary facts from electromagnetic scattering theory. In section 3, we discuss the issues of solving nonlinear equations and choosing the starting point. In section 4, we give the results of numerical experiments.

## 2. Direct and inverse scattering problem for small particles

### 2.1. Scattering problem

As is well known, propagation of time-harmonic electromagnetic waves is described by the Maxwell equations

$$\operatorname{curl} \mathbf{E}(x) = i\omega\mu\mathbf{H}(x), \quad (3)$$

$$\operatorname{curl} \mathbf{H}(x) = -i\omega\varepsilon\mathbf{E}(x), \quad x \in \mathbb{R}^3, \quad (4)$$

where  $\mathbf{E}$  and  $\mathbf{H}$  are the electric and magnetic fields,  $\omega$  is the frequency, and  $\varepsilon$  and  $\mu$  are the electric permittivity and magnetic permeability. We suppose that  $\mu$  is constant and  $\varepsilon(x)$  is piecewise constant:

$$\varepsilon(x) = \begin{cases} \varepsilon_1 & \text{in } \Omega, \\ \varepsilon_0 & \text{outside } \Omega, \end{cases} \quad (5)$$

where  $\Omega$  is a bounded domain with a smooth boundary occupied by the particle.

The direct scattering problem is to find a solution of the form  $\mathbf{E}(x) = \mathbf{E}^{(i)}(x) + \mathbf{E}^{(s)}(x)$ , where the incident wave  $\mathbf{E}^{(i)}(x)$  satisfies (3) and (4) with  $\varepsilon \equiv \varepsilon_0$  and the scattered wave  $\mathbf{E}^{(s)}(x)$  meets the radiation condition (see [3]). Here and in the following, we consider only the electric field, since  $\mathbf{H}(x)$  is reconstructed from (3). As the incident wave, we take the plane wave  $\mathbf{E}^{(i)}(x) = \mathbf{E}^0 e^{ik\hat{e}^{(i)} \cdot x}$ , where  $\hat{e}^{(i)}$  is the unit vector in the incident direction,  $\mathbf{E}^0$  is a constant complex vector orthogonal to  $\hat{e}^{(i)}$  and  $k = \omega\sqrt{\varepsilon_0\mu}$  is the wavenumber connected with the wavelength  $\lambda$  by the relation  $k = \frac{2\pi}{\lambda}$ .

The scattered wave has the following asymptotic behavior at infinity:

$$\mathbf{E}^{(s)}(x) = \frac{e^{ik|x|}}{-ik|x|} \left( \mathbf{E}^\infty \left( \frac{x}{|x|} \right) + O\left(\frac{1}{|x|}\right) \right), \quad |x| \rightarrow \infty; \quad (6)$$

moreover,  $\mathbf{E}^\infty(\hat{x})$  is orthogonal to  $\hat{x}$  for every unit vector  $\hat{x} \in \mathbb{R}^3$ . In the spherical coordinates  $(r, \theta, \varphi)$ ,  $\mathbf{E}^\infty$  is a function of  $\theta$  and  $\varphi$ . Suppose that the incident direction coincides with the direction of the  $x_3$ -axis. For every direction  $(\theta, \varphi)$ , we standardly choose the basis  $\hat{e}_\perp^{(i)}, \hat{e}_\parallel^{(i)}$  in the  $x_1, x_2$ -plane and the basis  $\hat{e}_\perp^{(s)}, \hat{e}_\parallel^{(s)}$  in the tangent space to the sphere at the point  $(\theta, \varphi)$ , so that the first vector in each pair is perpendicular to the scattering plane and the second is parallel (for details see [4], section 3.2). Decompose the vectors  $\mathbf{E}^0$  and  $\mathbf{E}^\infty$  in the corresponding bases:

$$\mathbf{E}^0 = \mathbf{E}_\perp^0(\theta, \varphi)\hat{e}_\perp^{(i)} + \mathbf{E}_\parallel^0(\theta, \varphi)\hat{e}_\parallel^{(i)}, \quad (7)$$

$$\mathbf{E}^\infty(\theta, \varphi) = \mathbf{E}_\perp^\infty(\theta, \varphi)\hat{e}_\perp^{(s)} + \mathbf{E}_\parallel^\infty(\theta, \varphi)\hat{e}_\parallel^{(s)}. \quad (8)$$

In view of the linearity of the problem, the pairs of coefficients are connected as follows:

$$\begin{pmatrix} \mathbf{E}_\perp^\infty \\ \mathbf{E}_\parallel^\infty \end{pmatrix} = \begin{pmatrix} S_1(\theta, \varphi) & S_4(\theta, \varphi) \\ S_3(\theta, \varphi) & S_2(\theta, \varphi) \end{pmatrix} \begin{pmatrix} \mathbf{E}_\perp^0 \\ \mathbf{E}_\parallel^0 \end{pmatrix}. \quad (9)$$

The complex-valued matrix  $(S_p(\theta, \varphi))$  is called *the amplitude matrix*. The quadratic combinations of its entries constitute the Muller matrix  $S_{ij}(\theta, \varphi)$ ,  $i, j = 1, \dots, 4$ :

$$S_{11} = \frac{1}{2}(|S_1|^2 + |S_2|^2 + |S_3|^2 + |S_4|^2), \quad (10)$$

$$S_{12} = \frac{1}{2}(|S_2|^2 - |S_1|^2 + |S_4|^2 - |S_3|^2), \text{ etc.} \quad (11)$$

The real-valued functions  $S_{ij}(\theta, \varphi)$  are the most complete data that can be acquired in a real experiment.

## 2.2. The Mie theory (scattering by a homogeneous sphere)

In the case of a homogeneous sphere the scattered wave and the matrices can be written down explicitly. Below,  $\Omega$  is the sphere of radius  $a$ ,  $\alpha = ka$  is the size parameter,  $m = \sqrt{\frac{\varepsilon_1}{\varepsilon_0}}$  is the relative refraction index, and  $\beta = m\alpha$ .

The incident and scattered waves are expanded in the vector spherical harmonics  $\mathbf{M}_{p1n}^{(i)}, \mathbf{N}_{1pn}^{(i)}$ ,  $n = 1, 2, \dots$ , where  $p = e, o$  denotes parity (in  $\varphi$ ) and  $i$  takes the values 1 for regular harmonics and 3 for harmonics with the radiation condition (for details see, for example, [4], chapter 4):

$$\mathbf{E}^{(i)}(x) = E^0 \sum_{n=1}^{\infty} i^n \frac{2n+1}{n(n+1)} (\mathbf{M}_{o1n}^{(1)} - i\mathbf{N}_{e1n}^{(1)}), \quad (12)$$

$$\mathbf{E}^{(s)}(x) = E^0 \sum_{n=1}^{\infty} i^n \frac{2n+1}{n(n+1)} (ia_n \mathbf{N}_{e1n}^{(3)} - b_n \mathbf{M}_{o1n}^{(3)}). \quad (13)$$

The coefficients  $a_n$  and  $b_n$  are found from the condition of equality of the tangent components of the internal and external fields and have the form

$$a_n = \frac{m\psi_n(\beta)\psi'_n(\alpha) - \psi_n(\alpha)\psi'_n(\beta)}{m\psi_n(\beta)\xi'_n(\alpha) - \xi_n(\alpha)\psi'_n(\beta)}, \quad (14)$$

$$b_n = \frac{\psi_n(\beta)\psi'_n(\alpha) - m\psi_n(\alpha)\psi'_n(\beta)}{\psi_n(\beta)\xi'_n(\alpha) - m\xi_n(\alpha)\psi'_n(\beta)}, \quad n = 1, 2, \dots, \quad (15)$$

where  $\psi_n(\rho) = \rho j_n(\rho)$ ,  $\xi_n(\rho) = \rho h_n^{(1)}(\rho)$ ,  $h_n^{(1)}(\rho) = j_n(\rho) + iy_n(\rho)$ , and  $j_n(\rho)$  and  $y_n(\rho)$  are the spherical Bessel functions. For entries of the amplitude matrix, we obtain the expressions

$$S_1(\theta) = \sum_{n=1}^{\infty} \frac{2n+1}{n(n+1)} (a_n\pi_n(\theta) + b_n\tau_n(\theta)), \quad (16)$$

$$S_2(\theta) = \sum_{n=1}^{\infty} \frac{2n+1}{n(n+1)} (b_n\pi_n(\theta) + a_n\tau_n(\theta)), \quad (17)$$

$$S_3(\theta) = S_4(\theta) = 0, \quad (18)$$

where

$$\pi_n(\theta) = \frac{P_n^1(\cos\theta)}{\sin\theta}, \quad \tau_n(\theta) = \frac{dP_n^1(\cos\theta)}{d\theta}, \quad (19)$$

$P_n^m(t)$  are the associated Legendre polynomials.

Obviously, we can also obtain expressions for  $S_{ij}(\theta)$  in the form of infinite series in the products of  $\pi_n(\theta)$  and  $\tau_n(\theta)$ .

Thus, the solution of the direct problem assumes the following chain:

$$\alpha, m \longrightarrow a_n, b_n \longrightarrow S_i(\theta) \longrightarrow S_{ij}(\theta). \quad (20)$$

Differentiating (14) and (15), we can explicitly find the derivatives of  $S_{11}(\theta)$  with respect to  $\alpha$  and  $m$ .

### 2.3. Inverse Mie problem

The inverse problem is to find the size parameter  $\alpha$  (radius  $a$ ) and the refractive index  $m$  from  $S_{ij}(\theta)$  or  $S_i(\theta)$  given for some angles  $\theta \in [0^\circ, 180^\circ]$ .

The methods for solving the inverse Mie problem can be conditionally divided into empirical, analytical and optimization methods (we do not consider those based on various approximations).

*Empirical methods*, which come first historically, are based on the computation of (many) solutions to the direct problem and matching them to experimental data [5–8]. So, in [8], empirical formulas were given for  $a$  and  $m$  obtained from the analysis of the position of peaks of the LSP  $A(\theta)$  and its values at these points.

*Analytical methods* assume theoretical analysis of the direct map and obtain a formula or algorithm. It turns out that the coefficients in the Fourier expansion of  $A(\theta)$  or the expansion in orthogonal polynomials (for example, Gegenbauer polynomials) exhibit a specific behavior. Namely, the coefficients rapidly decrease beginning with a number which is explicitly connected with the size parameter and practically independent of  $m$  [9, 10]. This observation gives an inversion procedure for the size parameter. However, for rigorous implementation of this method, we need  $A(\theta)$  for all  $\theta \in [0^\circ, 180^\circ]$ .

We should observe in particular the purely analytical solution of the inverse Mie problem of [11]. Assume that  $S_i(\theta)$  is given for  $\theta \in [0^\circ, 180^\circ]$ . The coefficients  $a_n$  and  $b_n$  are easily found

from  $S_1(\theta)$  and  $S_2(\theta)$ , respectively, in view of the orthogonality of the families  $\pi_n(\theta) \pm \tau_n(\theta)$  by the formulas

$$a_n = \frac{1}{2n(n+1)} \int_0^\pi (S_2(\theta)\tau_n(\theta) + S_1(\theta)\pi_n(\theta)) \sin \theta \, d\theta, \quad (21)$$

$$b_n = \frac{1}{2n(n+1)} \int_0^\pi (S_2(\theta)\pi_n(\theta) + S_1(\theta)\tau_n(\theta)) \sin \theta \, d\theta. \quad (22)$$

Then  $\alpha$  and  $m$  are found for  $a_n$  and  $b_n$  as follows. Eliminating from (14) and (15) the values depending on  $\beta$ , we obtain the identity

$$m^2 = \frac{a_n \xi_n(\alpha) - \psi_n(\alpha) \quad b_n \xi_n'(\alpha) - \psi_n'(\alpha)}{a_n \xi_n'(\alpha) - \psi_n(\alpha) \quad b_n \xi_n(\alpha) - \psi_n(\alpha)}, \quad (23)$$

which is valid for  $n = 1, 2, \dots$ . Given  $a_n$  and  $b_n$ , consider the function  $f_n(z)$  equal to the right-hand side of (23) for  $\alpha = z$ . If  $z = \alpha$ , then the sequence  $f_n(z)$  is obviously constant and is equal to  $m^2$ . In [11], it was demonstrated that the converse is also true: the sequence is constant only for  $z = \alpha$ . Thus, the algorithm for finding  $\alpha$  and  $m$  assumes the construction of the sequence  $f_n(z)$  for different  $z$ s. The value of  $z$  for which  $f_n(z)$  is constant is the sought  $\alpha$  and the value  $f_n(z)$  equals  $m^2$ . Thus, we have an analytical inversion procedure for the first two steps in (20).

Now, we discuss the inversion of the last passage. At this step, we lose the information. In the general case from four complex-valued functions  $S_i(\theta, \varphi)$ , we obtain 16 functions  $S_{ij}(\theta, \varphi)$  of which only seven are independent. From these functions, we can reconstruct the absolute values  $|S_i(\theta, \varphi)|$  and the differences between their arguments. In the case of a sphere, only three of the functions  $S_{ij}(\theta)$  are independent. Thus, the inversion of the last step is hardly possible without *a priori* information about  $S_j$ . The authors are unaware of such results. Observe that most theoretical studies of the inverse scattering problems assume that  $S_i$  are given.

*Optimization methods.* In the case when  $S_{ij}(\theta)$  is given for a limited number of angles, one broadly uses optimization methods which are based on finding the (global) minimum of some (objective) residual functional, for example,

$$R(a, m) = \sum_{j=1}^m |A^p(\theta_j; a, m) - A_j^d|^2,$$

where  $A_j^d$  is the LSP measured at  $\theta_j$  and  $A^p(\theta; a, m)$  is the computed LSP of the particle with parameters  $a$  and  $m$ . Sometimes,  $A(\theta)$  is replaced with  $\log A(\theta)$  and weighted functionals are used. So optimization methods differ by the objective functional and the way of minimization: gradient and nongradient. Gradient methods need a good starting point and are local in this sense. An application of the gradient method to the inverse Mie problem is presented in [12], where local minimizations are repeatedly carried out with different starting points chosen according to the stochastic algorithm of Rinnooy Kan and Timmer [13, 14]. Note that in [12], unlike this paper, the starting points are constructed individually for each particle.

The basic nongradient method for global minimization used for solving the inverse Mie problem is the DIRECT method [15–17]. Its application to the particle sizing problem is described in [12, 18] (see also the bibliography therein).

*Neural networks.* There are several articles where the inverse Mie problem is solved by means of neural networks [19–22].

All existing methods have advantages and drawbacks. Empirical and neural network methods are not sufficiently rigorous. Purely analytical methods do not apply to real data. The most powerful practical methods are the optimization methods. Although they may

require unpredictably large amounts of computation. Observe that this amount depends on the range of the sought parameters. For example, small particles may require fewer iterations than large ones. The approach proposed in this paper can reduce the number of computations and predict for which particles the problem is better solved.

In conclusion, we give a list of recent works on close inverse scattering problems: [2, 23–26] (see also the bibliography therein).

### 3. Solution of a nonlinear equation

#### 3.1. Statement of the problem

Let  $f : X \rightarrow \mathbb{R}^d$  be a smooth function in a bounded domain  $X \subset \mathbb{R}^p$ . We suppose that the number of parameters  $p$  is small and the number of data  $d$  is rather large; anyway  $p < d$ . The parameter space  $\mathbb{R}^p$  is furnished with the inner product  $\langle \cdot, \cdot \rangle$  and the corresponding norm  $\| \cdot \|_p$  and the data space  $\mathbb{R}^d$ , with the norm  $\| \cdot \|_d$ . Let  $X_1$  be a subdomain of  $X$  whose boundary is distant from the boundary of  $X$ . Given  $y^0 = f(x^0)$ ,  $x^0 \in X_1$ , we need to find  $x^0$ . The following questions arise.

- (1) Does  $y^0$  uniquely determine  $x^0$ ?
- (2) How can we reconstruct practically  $x^0$  from  $y^0$  or its approximate value  $y^\delta$ ?
- (3) How is inaccuracy in  $y^0$  transformed into the error in  $x^0$ ?

We are mainly interested in the second question. Partial answers to the other two questions follow from the numerical results at the end of the paper.

If the equation  $f(x) = y^0$  has a unique solution, then it can be sought as the global minimum of the residual functional  $R_{y^0}(x) = \|f(x) - y^0\|_d^2$ . If we can compute the derivatives of  $f(x)$ , then it is reasonable to carry out minimization by a gradient method, for example, the conjugate gradient method, provided that the starting point is close enough to  $x^0$ . In the case when the equation  $f(x) = y^0$  is repeatedly solved with different data  $y^0$ , we can state the following problem.

**Problem 1.** Find a set  $\{z_j\}$  of starting points such that for every  $x^0 \in X_1$  there is at least one good starting point, i.e. a point  $z_j$  such that the minimization process for  $R_{y^0}(x)$  started at  $z_j$  leads to  $x^0$ .

Having constructed  $\{z_j\}$ , we can solve the equation  $f(x) = y^0$  with the indicated method for arbitrary data  $y^0 = f(x^0)$ ,  $x^0 \in X_1$ . However, if  $\{z_j\}$  is large, the following problem appears.

**Problem 2.** Suppose that  $\{z_j\}$  is constructed. Given  $y^0$ , find a (possibly small) subset of  $\{z_j\}$  such that at least one  $z_j$  in this subset leads to  $x^0$ .

We discuss these problems below.

#### 3.2. The set of starting points

For the constructions below, we introduce some functions on  $X_1$ . Fix  $x^0 \in X_1$  and consider the residual functional  $R_{y^0}(x)$ ,  $y^0 = f(x^0)$ . Define

$$r(x^0) = \sup\{r > 0 \mid B(x^0, r) \subset X \text{ and} \quad (24)$$

$$\forall x \in B(x^0, r) \langle \text{grad}_x R_{y^0}(x), x - x^0 \rangle < 0\}. \quad (25)$$

The value  $r(x^0)$  is the radius of the greatest ball for which at all interior points the direction of steepest descent ‘looks toward’  $x^0$ .

It is obvious that

- the point  $x^0$  is a unique local minimum of  $R_{y^0}(x)$  in  $B(x^0, r(x^0))$ ;
- the minimization process for  $R_{y^0}(x)$  started at an arbitrary point of  $B(x^0, r(x^0))$  leads to  $x^0$ ;
- the ball  $B(x^0, r(x^0))$  depends on the inner product (and the norm) in  $\mathbb{R}^p$  and may cover a greater or smaller part of all good starting points.

Estimate  $R_{y^0}(x)$  outside  $B(x^0, r(x^0))$  and put

$$t(x^0) = \inf_{x \in X_1 \setminus B(x^0, r(x^0))} R_{y^0}(x). \quad (26)$$

The value  $t(x^0)$  characterizes the uniqueness of the solution to the equation  $f(x) = y^0$ : if  $t(x^0) > 0$ , then  $x^0$  is uniquely determined by  $y^0$ . Define

$$s(x^0) = \sup\{s > 0 \mid \forall x \in B(x^0, s) R_{y^0}(x) < t(x^0)\}. \quad (27)$$

It is clear that the value  $R_{y^0}(x)$  at an arbitrary point  $x \in B(x^0, s(x^0))$  is less than every extraneous local minimum.

The set of starting points can be constructed in two ways.

**Method 1.** For a point  $z \in X_1$  consider all balls  $B(x, r(x))$ ,  $x \in X_1$ , containing  $z$ . Their centers  $x$  constitute the set of points for which  $z$  is a good starting point:

$$C(z) = \{x \in X_1 \mid z \in B(x, r(x))\}. \quad (28)$$

We call  $C(z)$  the cover zone of  $z$ .

Take  $z_1$  to be the point  $z \in X_1$  with the greatest  $\text{meas} C(z)$ . Suppose that the points  $z_1, \dots, z_k$  are already constructed. For  $z \in X_1 \setminus \cup_{j=1}^k C(z_j)$  define  $d_k(z)$  to be the distance from  $z$  to the domain already covered,  $\cup_{j=1}^k C(z_j)$ . The next point  $z_{k+1}$  is taken to be the one with the greatest value  $\min\{\pi d_k(z), \text{meas} C(z)\}$  (we multiply by  $\pi$  to get the disk area). This choice is a trade-off between having a large coverage area and being distant from the set of points already covered. Eventually, provided that  $r(x) > 0$  on  $X_1$ , we obtain a finite  $\{z_1, \dots, z_N\}$  such that  $X_1 \subset \cup_{j=1}^N C(z_j)$  (finiteness is a consequence of the Borel–Lebesgue theorem).

**Method 2.** The second method is similar to the first with the only difference that the balls  $B(x, r(x))$  are replaced with  $B(x, s(x))$ . Naturally, the set  $\{z_j\}$  constructed by the second method is greater. However, this method has advantages at the solution stage.

### 3.3. Solution of the equation

Suppose that the set of starting points  $\{z_j\}$  is constructed. Let  $y^0 = f(x^0)$ ,  $x^0 \in X_1$ , be given. For a common reason, we have to minimize the residual functional  $R_{y^0}(x)$  starting successively from every point  $z_j$  and then choose the result with least residual (zero in the case of exact data). However, the number of points  $z_j$  can be rather large. To optimize the process we do the following.

- Choose those points in  $\{z_j\}$  which may potentially lead to  $x^0$ .
- Arrange the selected points  $z_j$  by importance.
- Formulate the test for the solution constructed so far to be unimprovable (this is especially necessary for the solution of equations with the approximate right-hand side).

The strategy naturally depends on the method of construction of the set  $\{z_j\}$ .

**Method 1.** At the stage of construction of  $\{z_j\}$ , for every  $z_j$  we can compute the value

$$m(z_j) = \sup_{x \in C(z_j)} \|f(z_j) - f(x)\|_d. \quad (29)$$

Violation of the condition  $R_{y^0}(z_j) < m(z_j)$  means that  $x^0$  whose data might be  $y^0$  does not belong to the cover area  $z_j$  and hence we should not start with  $z_j$ . Thus, we choose the condition  $R_{y^0}(z_j) < m(z_j)$  for the selection of potentially good starting points  $z_j$ .

Then, we simply arrange  $z_j$  by the values  $R_{y^0}(z_j)$ . Note that the point with the least value of the residual functional may fail to be a good starting point for  $x^0$ .

**Method 2.** In the case of  $\{z_j\}$  constructed by the second method, we simply find  $z_k$  with the least value  $R_{y^0}(z_k)$ . By construction, the point  $z_k$  is necessarily a good starting point. Indeed, by construction among  $\{z_j\}$  there is at least one  $z_l \in B(x^0, s(x^0))$ . Then, we have the chain of inequalities  $R_{y^0}(z_k) \leq R_{y^0}(z_l) \leq t(x^0)$  which means that  $z_k \in B(x^0, s(x^0))$  is a good starting point.

### 3.4. Data with noise

In practice, the data are always corrupted with noise; that is, we have some approximation  $y^\delta$  of  $y^0$ . In this event, we can still apply our optimization approach, obtaining thereby the minimum point  $x^\delta$ . The following questions arise.

- (1) Can we still use the set  $\{z_j\}$  for finding the global minimum of  $R_{y^\delta}(x)$  as described above?
- (2) How do we estimate  $\|x^\delta - x^0\|_\rho$ , knowing  $\|y^\delta - y^0\|_d$ ?

Unfortunately, we cannot answer these questions theoretically. The results of numerical simulations below provide a partial answer.

## 4. Numerical experiments

We apply the described approach to the problem of finding the radius ( $a$ ) and refractive index ( $n_1$ ) of a homogeneous sphere from the scattering data  $A(\theta_j)$ , where the angles  $\theta_j$ ,  $j = 1, \dots, d$ ,  $d = 128$ , constitute a uniform grid from  $10^\circ$  to  $70^\circ$ . Below, we use the first method for the construction of the set of starting points and solution of the optimization problem.

### 4.1. Parameterization of particles

Besides the natural parameters  $\alpha$  and  $m$ , we use other parameterizations. In order to relate our range to the size of biological particles, we use the physical parameters  $r = \lambda\alpha/2\pi n_0$  and  $n_1 = mn_0$ , where  $\lambda$  is the wavelength in vacuum and  $n_0$  is the refractive index of the media. In our experiments  $\lambda = 0.66 \mu\text{m}$  and  $n_0 = 1.337$ .

Another parameterization uses the parameters  $\alpha$  and  $\rho = 2\alpha(m - 1)$ . The parameter  $\rho$  is sometimes called the *phase-shift parameter* [8]. The parameters  $\alpha$  and  $\rho$  are more convenient for the construction of the set of starting points and the solution of the inverse problem, since the partial derivatives of the LSP  $A(\theta)$  with respect to them have the same order.

The norm in the parameter space is defined as  $\|(\alpha, \rho)\|^2 = \alpha^2 + \rho^2$ , and the (weighted) norm in the data space is defined as  $\|A\|_w^2 = \frac{1}{d} \sum_{j=1}^d |A(\theta_j) w(\theta_j)|^2$  with the weight function

$$w(\theta) = \frac{1^\circ}{\theta} \exp(-2 \ln^2(\theta/54^\circ)), \quad 1^\circ = \frac{\pi}{180},$$

displayed in figure 1(a). In fact, we multiply  $A(\theta)$  by  $w(\theta)/\sqrt{d}$  and use the function  $I(\theta) = A(\theta)w(\theta)/\sqrt{d}$  with the standard  $L_2$  norm:

$$\|I\|^2 = \sum_{j=1}^d |I(\theta_j)|^2 = \sum_{j=1}^d \frac{|A(\theta_j)w(\theta_j)|^2}{d} = \|A\|_w^2.$$

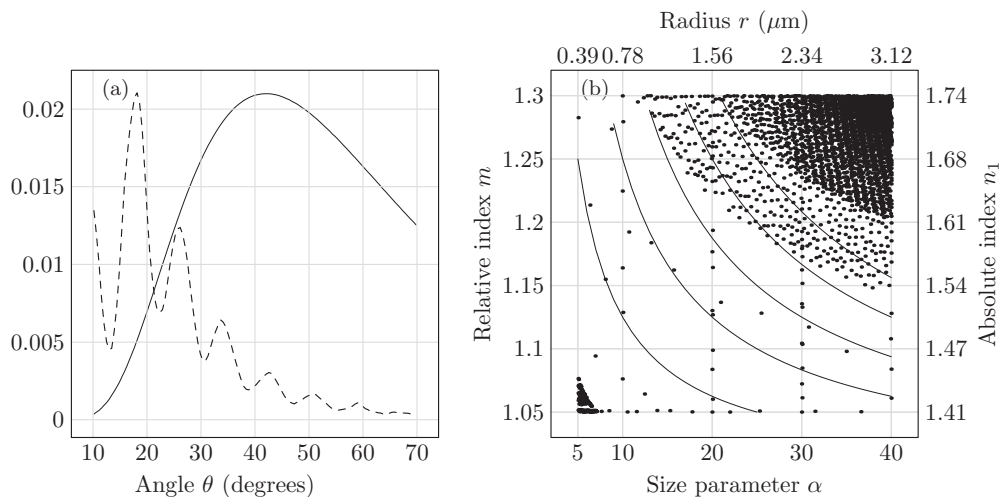


**Figure 1.** The weight function  $w(\theta)$  (solid line) and a typical experimental LSP (dashed line, no scale) (a) and the set of starting points (with isolines  $\rho = 2.5, \dots, 12.5$ ) (b).

The choice of  $w(\theta)$  is explained by the fact that the experimental data have more noise for angles close to  $10^\circ$  and  $70^\circ$  (see [27]).

#### 4.2. Starting points

The set of starting points is constructed for the domain  $X_1 = [5, 40] \times [1.05, 1.3]$  of parameters  $\alpha$  and  $m$  (see figure 1(b)). Since the solution of the inverse problem is carried out in the variables  $\alpha$  and  $\rho$ , we construct the starting points in these variables and then translate the result back into  $\alpha$  and  $m$ . Let  $\psi : (\alpha, m) \mapsto (\alpha, \rho)$ . Under the map  $\psi$ , rectangles get distorted; therefore, the construction, in fact, is carried out as follows. We split the domain  $X_1$  into subdomains  $X_1^k = [10k, 10(k+1)] \times [1.05, 1.3]$ , each of which is enclosed in a greater domain  $X^k = [10k-2, 10(k+1)+2] \times [1.01, 1.35]$ ,  $k = 0, \dots, 3$  (for  $k = 0$  the left endpoint is 5). For every  $X^k$ , we take the least rectangle  $G^k$  in the  $\alpha, \rho$ -space containing  $\psi(X^k)$ . Precompute the values  $S_{11}(\theta_j)$  and the derivatives in  $\alpha$  and  $\rho$  at the nodes  $(\alpha_i, \rho_k)$ ,  $i = 1, \dots, 200$ ,  $k = 1, \dots, 400$ , of the uniform grid for  $G^k$  and construct the set of starting points for the domain  $\psi(X_1^k)$  as described in the previous section. Finally, we take the union of the sets obtained for the subdomains. This method of construction leads to a small number of redundant points for  $\alpha \approx 10, 20, 30$ . The constructed set comprises 2458 points.

It is seen that the points have a nonuniform distribution, and their density increases with the growth of  $\rho$ . This is explained by the fact that for large  $\rho$ , the LSP  $I(\theta)$  oscillates fast and irregularly in  $\alpha$  and  $\rho$ . This phenomenon is well known under the name ripple structure (see [4], section 11.4). Another condensation of starting points is observed for small  $\alpha$  and  $m$ . We can see its part in the lower-left corner. This is explained by the fact that for small  $\alpha$  and  $m$  the LSP  $I(\theta)$  depends practically only on the parameter  $\rho$ , which leads to low resolution in the determination of  $\alpha$  and  $m$ .

#### 4.3. Exact synthetic data for spheres

We check the algorithm for exact synthetic data. The values  $I(\theta_j)$  are computed for 1000 random points  $(\alpha^0, m^0)$  in the domain  $X_1 = [5, 40] \times [1.05, 1.3]$ . These data are inverted by

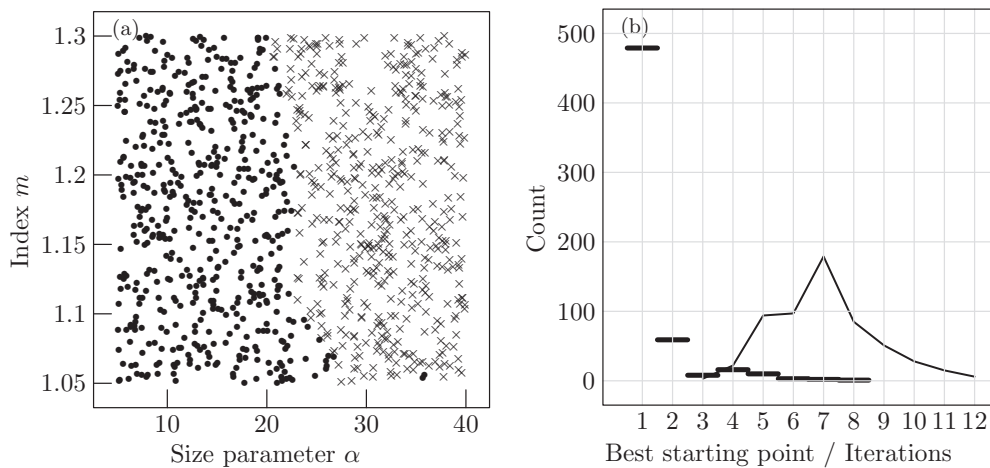


**Figure 2.** Checking the algorithm with exact data. The particles recovered from their LSP are dots and not recovered are crosses (a); the number of the best starting point (bars) and the number of iterations from the best starting point (line) for particles recovered from their LSP (b).

our algorithm with the set of starting points for the smaller domain  $X_0 = [5, 20] \times [1.05, 1.3]$ . The so-obtained solutions  $(\alpha^1, m^1)$  are compared with the exact parameters  $(\alpha^0, m^0)$  in the norm  $\|(\alpha, m)\|^2 = \alpha^2 + 100m^2$ . In figure 2(a), the points  $(\alpha^0, m^0)$  for which the difference is less than 0.001 are shown as dots, and the other points as crosses. It is well observed that all points of the domain for which the set of starting points was constructed are exactly determined by our method. However, the algorithm does not work for the points at some distance from  $X_0$ . It means that the choice of the starting point in the problem under consideration is important. In figure 2(b), we give the distribution of the numbers of the best starting points, that is, the starting points which lead to the global minimum, and the number of iterations from the best starting point to the solution. In most cases, the best starting point is the one with the least initial residual; it is also seen that the first eight points with the least initial residual are enough to find the global minimum.

#### 4.4. Noisy synthetic data for spheres

We study the stability of the solution under perturbation of data. Consider two types of errors: white noise and the systematic error connected with nonsphericity (see the next subsection).

In the first case, the LSPs  $I(\theta_j)$  of the points  $(\alpha^0, m^0)$  used in the first experiment are contaminated with Gaussian noise. The deviation is the same for all points of each LSP but different for different LSPs; namely it equals  $\left(\sum_{j=1}^{128} \frac{I(\theta_j)^2}{128}\right) \frac{q}{2}$ , where  $q$  is a random value with uniform distribution in  $[0, 0.2]$  chosen for each LSP. Figures 3(a) and (b) show the errors  $|\alpha^1 - \alpha^0|$  and  $|m^1 - m^0|$  versus the residual  $\frac{\|I^d - I^p\|}{\|I^d\|} \times 100\%$ , where  $I^d$  is the given LSP and  $I^p$  is the LSP of the found spherical particle. Observe that the errors increase regularly with the residual up to  $\approx 17\%$  (the bold dots in figures 3(a) and (b) stand for points with  $|\alpha^1 - \alpha^0| > 1$  or  $|m^1 - m^0| > 0.02$ ). The distribution of  $m^1 - m^0$  versus  $\alpha^1 - \alpha^0$  is shown in figure 3(c).

#### 4.5. Exact synthetic data for spheroids

In this case the data are generated as follows. We take a random pair  $(\alpha^0, m^0) \in [5, 40] \times [1.05, 1.3]$  (uniformly). For  $\alpha^0$ , we find a spheroid of the same volume as the sphere of radius

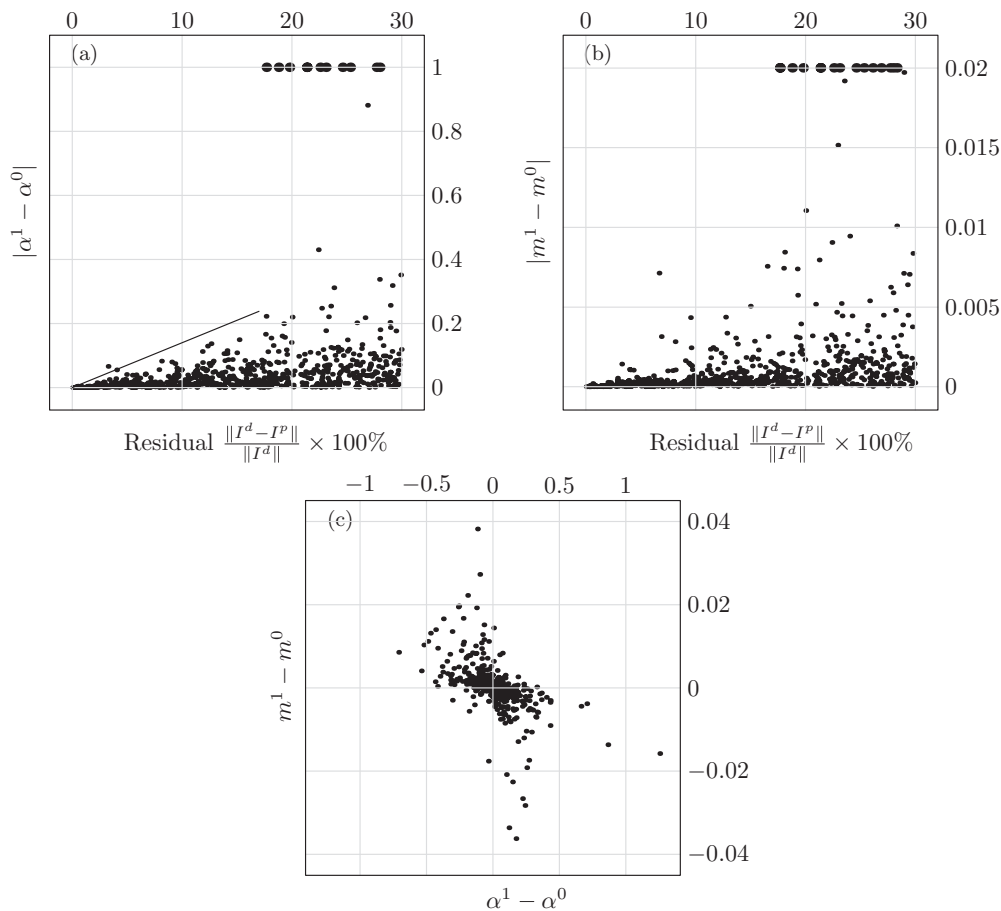


**Figure 3.** Stability of solution under perturbation of data with Gaussian noise: errors in  $\alpha$  and  $m$  versus the residual (a) and (b) (bold dots stand for points with  $|\alpha^1 - \alpha^0| > 1$  or  $|m^1 - m^0| > 0.02$ ), and the error in  $m$  versus the error in  $\alpha$  (c).

$\alpha^0$  with the uniformly random ratio of the axes in the interval  $(0.9, 1.1)$  and the random angle between the principal axis and the incident direction in the interval  $(0^\circ, 90^\circ)$ . For this spheroid, using the  $T$ -matrix method (see [28]) we find the LSP  $I(\theta_j)$  at 128 points  $\theta_j$  in the interval  $(10^\circ, 70^\circ)$ . The number of particles equals 1000.

After inversion we obtain the pair  $(\alpha^1, m^1)$ . In figures 4(a) and (b), we give the plots of the errors  $|\alpha^1 - \alpha^0|$  and  $|m^1 - m^0|$  versus the residual  $(\|I^d - I^p\|/\|I^d\|) \times 100\%$ , where  $I^d$  is the given LSP and  $I^p$  is the LSP of the spherical particle found (the bold dots in figure 4(b) stand for points with  $|m^1 - m^0| > 0.02$ ). In figures 4(c) and (d), we give the plots of  $|\alpha^1 - \alpha^0|$  and  $|m^1 - m^0|$  versus the nonsphericity factor  $e = \left| \frac{\text{principalaxis}}{\text{minoraxis}} - 1 \right|$ . These figures demonstrate good stability of the LSP and the method under nonspherical perturbation of data.

Finally, we make the following observation (see figure 4(f)). As a rule, the absolute error in  $m$  does not exceed  $0.1(m^1 - 1)$  independent of  $e$ . A similar assertion about  $\alpha$  does not take place.

In table 1, we give the mean absolute errors of  $\alpha$  and  $m$  of figures 3(c) and 4(e).

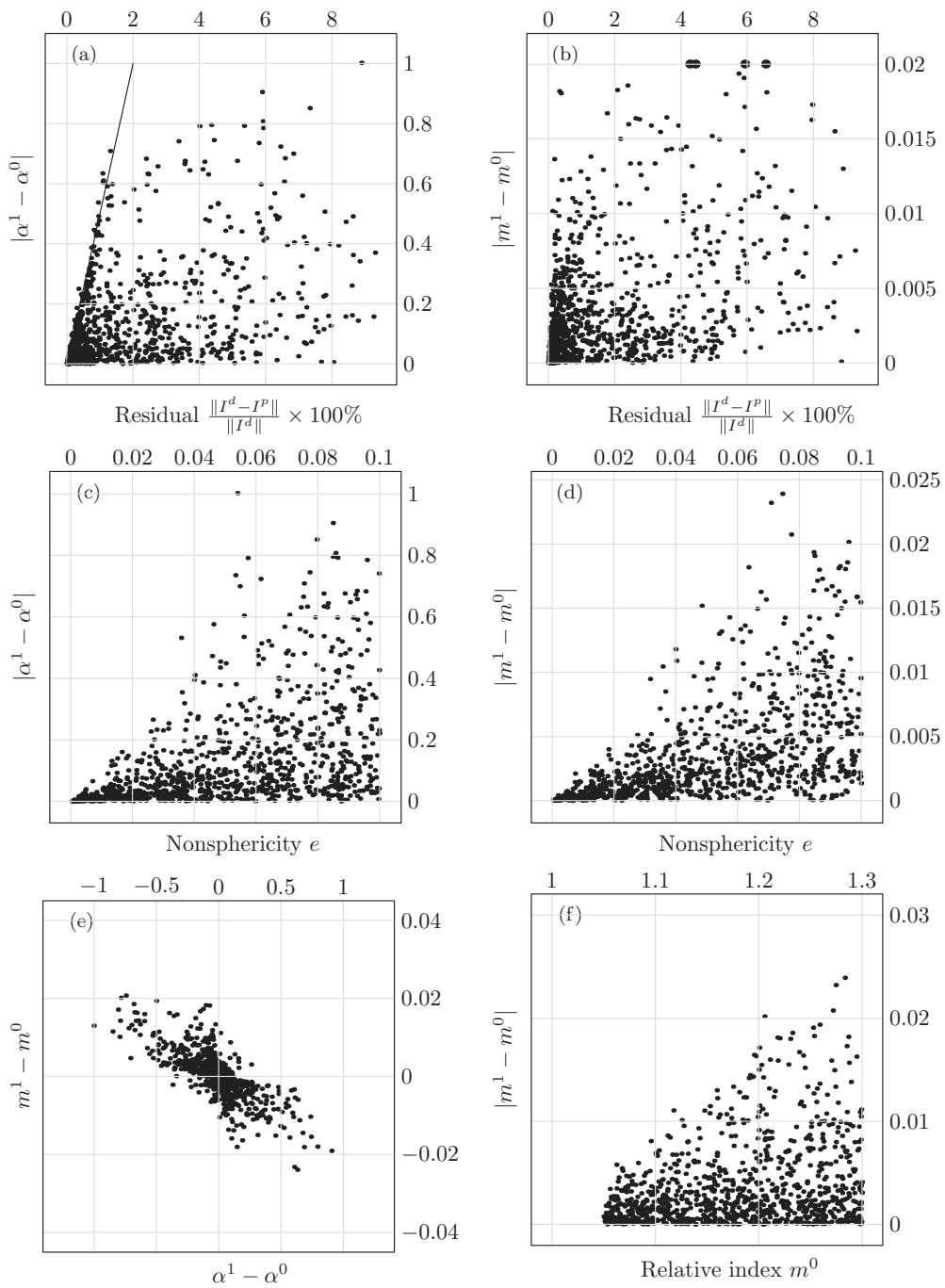


**Figure 4.** Stability of solution under nonspherical perturbation of data: errors in  $\alpha$  and  $m$  versus the residual (a) and (b) (bold dots stand for points with  $|\alpha^1 - \alpha^0| > 1$  or  $|m^1 - m^0| > 0.02$ ); errors in  $\alpha$  and  $m$  versus the nonsphericity  $e$  (c) and (d); error in  $m$  versus the error in  $\alpha$  (e); error in  $m$  versus  $m^0$  (f).

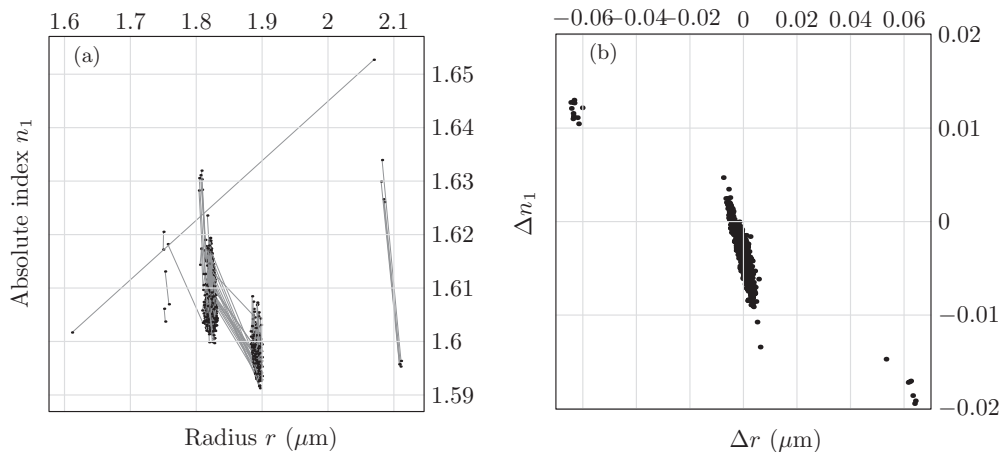


**Figure 5.** Inversion of experimental data. The solutions obtained by our method and the DIRECT method are connected by a segment (a);  $\Delta n_1$  versus  $\Delta r$  (b). The mean values of  $r$  and  $n_1$  are  $1.844 \mu\text{m}$  and  $1.603$ . The mean absolute errors in  $r$  and  $n_1$  are  $0.0038 \mu\text{m}$  and  $0.0038$ .

**Table 1.** Mean absolute errors.

|                   | Noisy spheres <sup>a</sup> | Ideal spheroids |
|-------------------|----------------------------|-----------------|
| Error in $\alpha$ | 0.15                       | 0.165           |
| Error in $m$      | 0.0057                     | 0.0058          |

<sup>a</sup> Taking the average, we drop the few particles with  $|\alpha^1 - \alpha^0| > 1$  or  $|m^1 - m^0| > 0.02$  for which the algorithm failed.

#### 4.6. Experimental data for polystyrene spheres

The experimental data  $I(\theta_j)$ ,  $j = 1, \dots, 128$ , were acquired using the scanning flow cytometer for 751 polystyrene particles. The particles are practically spherical in shape. According to the producer's data, the mean radius  $r$  is  $1.964 \mu\text{m}$  ( $\alpha = 25$ )  $\pm 4\%$ . The absolute refractive index  $n_1$  of bulk polystyrene at  $\lambda = 0.66 \mu\text{m}$  equals  $1.185$  ( $m = 1.58$ ). Since the exact parameters in this case are unknown, to verify the results, we processed the same data by another method. Namely, we used the optimization method in which the residual is minimized by means of the global search method DIRECT (see [15–17]). Figure 5(a) shows the parameters  $r$  and  $n_1$  of particles found by both methods. The corresponding points are connected by segments. Figure 5(b) shows the difference  $\Delta n_1$  in  $n_1$  versus the difference  $\Delta r$  in  $r$ .

## 5. Conclusion

In this paper, we propose an algorithm for the numerical solution of the inverse Mie problem with data acquired using a scanning flow cytometer. The problem reduces to the analysis of a strongly nonlinear map of finite-dimensional spaces. The algorithm comprises two parts.

- The preliminary part consists in the analysis of the direct map and its partial derivatives and construction of the set of good starting points. As a byproduct we find the domain in the parameter space where the problem can be solved in practice. The routines of this part

of the algorithm require a large amount of computation but need to be carried out only once for a particular type of direct map.

- Inversion of particular scattering data by the optimization method with the minimization of the residual functional by a gradient method using the constructed set of starting points.

Numerical experiments show that the second part requires minimum computations (see figure 2(b)).

Observe that implementation of this approach requires knowledge of the partial derivatives of the direct map. In the case of the Mie, they are found by explicit formulas.

Apparently, our approach can be used for the solution of the inverse scattering problem with a greater number of parameters (for example, for coated spherical particles or nonspherical particles with partial symmetry).

## Acknowledgments

This work was supported by integration grants of the Siberian Branch of Russian Academy of Science, nos 2009-37 and 2009-7, grant from the program of Presidium of the Russian Academy of Science, no 2009-27-15, grant from the Novosibirsk City Hall for young scientists, no 3210, and program of the Russian Government ‘Research and Educational Personnel of Innovative Russia at 2009-2013’ (contracts P1039, P422, P2497, 14.740.11.0729).

## References

- [1] Maltsev V P and Semyanov K A 2004 *Characterization of Bio-Particles from Light Scattering (Inverse and Ill-Posed Problems Series vol 47)* (Utrecht: VSP)
- [2] Chaumet P C and Belkebir K 2009 Three-dimensional reconstruction from real data using a conjugate gradient-coupled dipole method *Inverse Problems* **25** 024003
- [3] Colton D and Kress R 1998 *Inverse Acoustic and Electromagnetic Scattering Theory* (Berlin: Springer)
- [4] Bohren C F and Huffman D R 1983 *Absorption and Scattering Light by Small Particles* (New York: Wiley)
- [5] Wyatt P J 1980 Some chemical, physical and optical properties of fly ash particles *Appl. Opt.* **7** 975
- [6] Ulanowski Z J and Ludlow I K 1989 Water distribution, size and wall thickness in *Lycoperdon pyriforme* spores *Mycological Res.* **93** 28
- [7] Quist G M and Wyatt P J 1985 Empirical solution to the inverse light scattering problem by the optical strip-map technique *J. Opt. Soc. Am. A* **2** 1979
- [8] Maltsev V P and Lopatin V N 1997 Parametric solution of the inverse light-scattering problem for individual spherical particles *Appl. Opt.* **36** 6102–8
- [9] Ludlow I K and Everitt J 1995 Application of Gegenbauer analysis to light scattering from spheres: theory *Phys. Rev. E* **51** 2516
- [10] Ludlow I K and Everitt J 1996 Systematic behaviour of the Mie scattering coefficients of spheres as a function of order *Phys. Rev. E* **53** 2909
- [11] Ludlow I K and Everitt J 2000 Inverse Mie problem *J. Opt. Soc. Am. A* **17**
- [12] Zakovic S, Ulanowski Z J and Bartholomew-Biggs M C 1998 Application of global optimization to particle identification using light scattering *Inverse Problems* **14** 1053
- [13] Rinnooy Kan A and Timmer G T 1987 Stochastic global optimization methods: part I. Clustering methods *Math. Program.* **39** 27
- [14] Rinnooy Kan A and Timmer G T 1987 Stochastic global optimization methods: part II. Multilevel methods *Math. Program.* **39** 57
- [15] Jones D R, Perttunen C D and Stuckman B E 1993 Lipschitzian optimization without the Lipschitz constant *J. Optim. Theory Appl.* **79** 157–81
- [16] Gablonsky J M 2001 Direct version 2.0 user guide *Technical Report* CRSC-TR01-08 Center for Research in Scientific Computation, North Carolina State University <http://www.ncsu.edu/crsc/reports/ftp/pdf/crsc-tr01-08.pdf>
- [17] Finkel D E 2003 DIRECT optimization algorithm user guide, Center for Research in Scientific Computation, North Carolina State University [http://www4.ncsu.edu/~ctk/Finkel\\_Direct/DirectUserGuide\\_pdf.pdf](http://www4.ncsu.edu/~ctk/Finkel_Direct/DirectUserGuide_pdf.pdf)

- [18] Bartholomew-Biggs M C, Ulanowski Z J and Zakovic S 2005 Using global optimization for a microparticle identification problem with noisy data *J. Global Optim.* **32** 325–47
- [19] Nascimento C A O, Guardani R and Giulietti M 1997 Use of neural networks in the analysis of particle size distributions by laser diffraction *Powder Technol.* **90** 89
- [20] Hull P G and Quinby-Hunt M 1997 A neural-network to extract size parameter from light-scattering data *Proc. SPIE* **2963** 448
- [21] Ulanowski Z J, Wang Z, Kaye P H and Ludlow I K 1998 Application of neural networks to the inverse light scattering problem from spheres *Appl. Opt.* **37** 4027–33
- [22] Berdnik V V and Loiko V A 2009 Retrieval of size and refractive index of spherical particles by multiangle light scattering: neural network method application *Appl. Opt.* **48** 6178–87
- [23] Bassrei A and Lemaire T J 2007 Three-dimensional reconstruction of non-homogeneous dielectric objects by the coupled-dipole method *Braz. J. Phys.* **37** 325
- [24] Giacomelli M G, Chalut K J, Ostrander J H and Wax A 2009 Review of the application of T-matrix calculations for determining the structure of cell nuclei with angle-resolved light scattering measurements *IEEE J. Sel. Top. Quantum Electron.* **4** 900–8
- [25] Jaffe J S 2007 A tomographic approach to inverse Mie particle characterization from scattered light *Opt. Express* **15** 12217
- [26] Li W and Jaffe J S 2010 Sizing Mie particles from intensity-only angular scatter *J. Opt. Soc. Am. A* **27** 151–8
- [27] Strokotov D I, Yurkin M A, Gilev K V, van Bockstaele D R, Hoekstra A G, Rubtsov N B and Maltsev V P 2009 Is there a difference between T- and B-lymphocyte morphology? *J. Biomed. Opt.* **14** 064036
- [28] Mishchenko M I, Travis L D and Lacis A A 2002 *Scattering, Absorption, and Emission of Light by Small Particles* (Cambridge: Cambridge University Press)